Appl Phys B (2011) 102: 417–423
DOI 10.1007/s00340-010-4266-5

Applied Physics B
Lasers and Optics

Simultaneous measurements of atmospheric HONO and NO_2 via absorption spectroscopy using tunable mid-infrared continuous-wave quantum cascade lasers

B.H. Lee · E.C. Wood · M.S. Zahniser · J.B. McManus · D.D. Nelson · S.C. Herndon · G.W. Santoni · S.C. Wofsy · J.W. Munger

Received: 11 June 2010 / Revised version: 7 September 2010 / Published online: 20 October 2010
© Springer-Verlag 2010

Abstract Nitrous acid (HONO) is important as a significant source of hydroxyl radical (OH) in the troposphere and as a potent indoor air pollutant. It is thought to be generated in both environments via heterogeneous reactions involving nitrogen dioxide (NO_2). In order to enable fast-response HONO detection suitable for eddy-covariance flux measurements and to provide a direct method that avoids interferences associated with derivatization, we have developed a 2-channel tunable infrared laser differential absorption spectrometer (TILDAS) capable of simultaneous high-frequency measurements of HONO and NO_2. Beams from two mid-infrared continuous-wave mode quantum cascade lasers (cw-QCLs) traverse separate 210 m paths through a multi-pass astigmatic sampling cell at reduced pressure for the direct detection of HONO (1660 cm^{-1}) and NO_2 (1604 cm^{-1}). The resulting one-second detection limits ($S/N = 3$) are 300 and 30 ppt (pmol/mol) for HONO and NO_2, respectively. Our HONO quantification is based on revised line-strengths and peak positions for *cis*-HONO in the 6-micron spectral region that were derived from laboratory measurements. An essential component of ambient HONO measurements is the inlet system and we demonstrate that heated surfaces and reduced pressure minimize sampling artifacts.

B.H. Lee (✉) · G.W. Santoni · S.C. Wofsy · J.W. Munger
School of Engineering and Applied Sciences, Harvard University, Cambridge, MA, USA
e-mail: hwanlee@fas.harvard.edu

E.C. Wood · M.S. Zahniser · J.B. McManus · D.D. Nelson · S.C. Herndon
Center for Atmospheric and Environmental Chemistry, Aerodyne Research, Inc., Billerica, MA, USA

1 Introduction

Atmospheric nitrous acid (HONO) photo-dissociates with a lifetime between 10 and 20 minutes to yield nitric oxide (NO) and hydroxyl radical (OH), the main oxidant in the atmosphere. Nighttime HONO formation and photolysis at sunrise can contribute significantly to early morning photo-chemistry. Observations of mid-day HONO concentrations above levels expected from photo-stationary balance between HONO, NO and OH suggest a yet unidentified light-dependent production mechanism. These measurements have used various instruments in a wide range of environments [1–3]. Thus, HONO may make a larger contribution to the HO_x ($= OH + HO_2$) cycle in the lower troposphere than has been accounted for by its nighttime formation. In addition, HONO chemistry may contribute to reactivating deposited nitrogen, which was presumed to be permanently removed from photo-chemical cycle. HONO is also an indoor air pollutant—both emitted directly from combustion processes and formed on various surfaces—and can react with amines to form carcinogenic compounds [4, 5]. NO_2 is proposed as a precursor to HONO formation via heterogeneous reactions. In order to examine the exchange of HONO between the biosphere and atmosphere and the role of NO_2 in this exchange, we have developed a dual-laser spectrometer to simultaneously measure both gases.

Several factors make accurate HONO measurements difficult. It is unstable, so certified reference gases for HONO do not exist. Its reactivity and solubility also make it prone to sampling losses and artifacts. Consequently, intercomparisons between different techniques often exhibit significant discrepancies [2, 6]. Further progress on understanding HONO sources and sinks requires a sensitive and unambiguous measurement method.

There are many methods to detect HONO, but they do not fully satisfy the need for sensitivity, selectivity and fast time response. Analytical techniques based on derivatization partition gaseous HONO into a liquid and subsequently measure the nitrite ion or its derivative by ion or liquid chromatography, long-path photometry or chemiluminescence [4, 7–9]. Although these methods can be very sensitive, the need to scrub HONO into solution may introduce sensitivity to any other gas-phase species that react with the solution [6]. Such interferences can be corrected if the chemically active species is quantifiable [10]. Furthermore, the need for long extraction integration times (a few minutes) precludes the application of these methods to eddy-covariance flux measurements.

Absorption spectroscopy directly measures atmospheric trace gases without the need for chemical extraction, with calibrations that are based on constant absorption cross-sections (line-strengths) and specificity that can be confirmed by spectral identification. However, absorption spectroscopic analytical methods tend to be expensive, and for many trace gases the fundamental sensitivity is relatively low, requiring either long absorption paths or increased signal averaging time. Both open-path (differential optical absorption spectroscopy, DOAS) [1, 11, 12] and closed-path (tunable diode laser absorption spectroscopy, TDLAS) [13, 14] systems have been utilized to measure HONO. Based on a prior implementation of nitric acid (HNO_3) and NO_2 TDLAS [15–17], we have developed a dual-channel tunable infrared laser differential absorption spectrometer (TILDAS) using continuous-wave quantum-cascade lasers instead of diode lasers to measure HONO and NO_2. The advantages of using cw-QC lasers in TILDAS over diode lasers in TDLAS are greater mode stability, higher laser power output and the ability to operate both lasers and detectors near room temperature without the need for cryogenic cooling, which facilitates long-term field measurements. The spectrometer is coupled with sample handling and calibration schemes intended to minimize inlet artifacts and provide quality-assurance that the system is working properly. Section 2 describes the spectrometer design and quantifies performance. Section 3 presents results from the investigation of HONO line-strengths and peak positions. Section 4 describes the sampling scheme and presents preliminary results from field measurements demonstrating the absence of positive and negative artifacts.

2 Instrument

The main components of the optical table (Fig. 1) include two light sources, a reference cell, multi-pass sampling cell and two detectors. For the light source, the spectrometer uses two thermo-electrically cooled QC lasers (Alpes Lasers) operated in continuous-wave mode that output light in the 6-micron spectral region. The laser light is scanned across a frequency spectrum in time by controlling its temperature, which is coarsely tuned with a Peltier element and finely tuned on a milli-Kelvin scale by providing the lasers with a programmable current ramp using a high compliance current source (ILX Lightwave). The resulting laser frequency scan covers approximately 0.2 cm^{-1} with a resolution of about 0.001 cm^{-1} per channel. The instrumental line-widths for both lasers are less than 0.001 cm^{-1} (half-width at half-maximum), which is smaller than Doppler broadened widths. The tuning rates of each laser are determined with a germanium etalon.

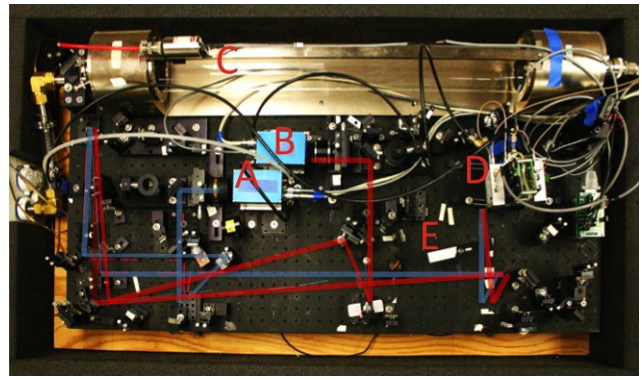

Fig. 1 Optical table of the dual cw-QC laser spectrometer. **A** = QC laser (1660 cm^{-1}, HONO); **B** = QC laser (1604 cm^{-1}, NO_2); **C** = astigmatic multi-pass sampling cell; **D** = thermo-electrically cooled detector; **E** = reference cell filled with NO_2 and HONO. The *blue* and *red traces* represent paths traveled by the HONO (1660 cm^{-1}) and NO_2 (1604 cm^{-1}) laser light, respectively. The traces for the reference cell and normalization are not shown. The optical table has a footprint of 2 ft × 4 ft (0.6 m × 1.2 m)

The two lasers are spatially and temporally multiplexed so that even though light from each laser traverses distinct paths inside and outside the sampling cell, both beams are collected by a single detector at alternate times on the order of 1 ms for each laser. The spectra for NO_2 (1604.5 to 1604.7 cm^{-1}) and HONO (1659.5 to 1659.7 cm^{-1}) are repeatedly scanned one after the other at a total rate of about 3 kHz and are subsequently averaged in real-time to improve the signal to noise ratio. Approximately 10% of the duty cycle is dedicated to measuring the detector zero light level when both lasers are off. The spectral fitting software (TDLWintel, also responsible for the laser control) determines the absorbance by performing a non-linear fit according to a set of Voigt line shape functions to the recorded spectra and a low-order polynomial fit to the spectral baseline. Mixing ratios are calculated by accounting for the sample pressure and temperature along with spectral broadening and IR line-strengths archived in the HITRAN database for NO_2 [18] and determined experimentally here for HONO (discussed below). Figure 2 shows transmission

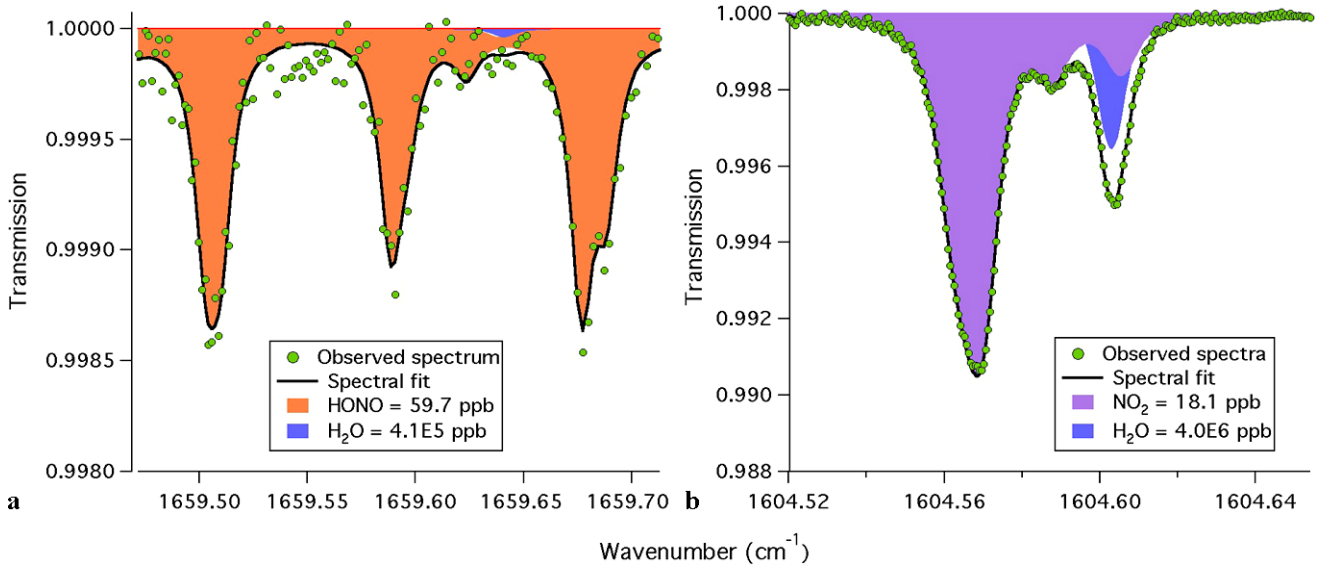

Fig. 2 Transmission spectra, averaged over 30-seconds, of (**a**) HONO and (**b**) NO_2 at 40 torr. The *colored areas* represent the fits to the observed spectra (*green dots*) according to the known peak position, line-strength and recorded pressure and temperature

spectra of HONO and NO_2 observed during calibration gas additions.

Ambient air is sampled through an inlet and transported in tubing (discussed below) to the sampling cell, which is maintained at a constant reduced pressure to minimize spectral overlap with other infrared-light absorbing species (especially water), while maintaining sufficient absorption depths for high sensitivity. Light from each laser enters the multi-pass cell and reflects between two astigmatic mirrors with multilayer dielectric coatings (reflectivity ~0.998, LohnStar Optics, Inc.). The mirrors are spaced 0.88 m apart and obtain 238 passes, resulting in a total path-length of 210 m. The light exits the cell through the entrance coupling-hole and is directed onto a thermo-electrically cooled detector (Vigo). It should be noted that a liquid-nitrogen cooled HgCdTe detector—which, due to its larger active detector area, is less susceptible to aiming changes—could be used to improve overall stability. However, the costs and measurement interruptions associated with liquid nitrogen fills for a comparable level of sensitivity with the HgCdTe detectors, make the thermo-electrically cooled detectors a preferred option.

The optical table also includes secondary and tertiary light paths, both external to the sampling cell—derived from the reflections off the front and back surfaces of a transmission beam splitter. One path is directed through a 7 cm path-length reference cell filled with gaseous HONO and NO_2. The spectra of this transmitted light is continuously measured by a second detector and is used to "lock" the lasers to the desired absorption features of HONO and NO_2, which is necessary when ambient levels of the species of interest are too low to observe significant absorbance in real-time and also preferred for the routine additions of zero-air, or ambient air scrubbed of these gases. The third beam and detector could be used to normalize out power variability associated with the light source, if desired, but has not been implemented. Details regarding the laser control, optical trace and alignment, data acquisition system, spectral fitting software, detectors and sampling cell have been discussed at length previously [17, 19–22].

Absorbance precisions less than 3×10^{-6} $Hz^{-1/2}$ (1.4×10^{-10} $cm^{-1}\,Hz^{-1/2}$) and 5×10^{-6} $Hz^{-1/2}$ (1.9×10^{-10} $cm^{-1}\,Hz^{-1/2}$) are achieved for HONO and NO_2, respectively. The NO_2 channel is slightly noisier due to the inherent variability of this particular QC device. We achieve the same absorbance precision as that of HONO by utilizing normalization [22]. Normalization with intermittent peak-position locking could be implemented in this dual detector configuration, however, it does not improve HONO sensitivity. Furthermore, at the low HONO mixing ratios expected in rural environments, intermittent line-locking is not adequate to maintain the laser tuning. We sacrifice some NO_2 sensitivity, which is not needed for typical ambient NO_2 levels, to ensure accurate HONO spectroscopy. For measurements at cell pressure of 40 torr, the one-second $1-\sigma$ precisions for HONO and NO_2 are 100 and 10 ppt (6 ppt if absorbance precision observed for HONO is achieved for NO_2), respectively. Long-term stability is limited by optical fringes that change with temperature, causing drifts in the spectral baseline. These effects may be minimized by frequent background spectrum subtractions obtained by flushing the cell with HONO and NO_2

scrubbed air, or zero-air, which is generated by passing ambient air over a heated palladium catalyst. This source of zero-air does not significantly alter the water-vapor mixing ratio, which is critical because there are weakly absorbing H_2O features in both the HONO and NO_2 scans (Fig. 2). Time averaging improves the precision of HONO and NO_2 measurements by a factor of 10 or better over an integration time of 30 minutes, which is a typical interval to compute eddy covariance over a forest canopy, with background spectra subtractions conducted once every 5 minutes (Fig. 3).

An optimal spectral region is selected based upon the maximum absorption cross-section and minimum absorbance by other gases that may be present in the sample. We selected the 6-micron region (Fig. 2) where lasers, detectors and mirrors were all available allowing simultaneous measurements of HONO and NO_2. There are, however, alternative spectral regions where HONO absorbs mid-infrared light much more strongly, which may improve sensitivity. In particular, HONO absorption lines at 1708.998, 1713.511, 1247.165 and 1273.598 cm^{-1} may increase precision by a factor of three to five, however, the 8.0 micron region would be costly for NO_2 measurement sensitivity and at this time no appropriate lasers are available in the 5.8 micron region.

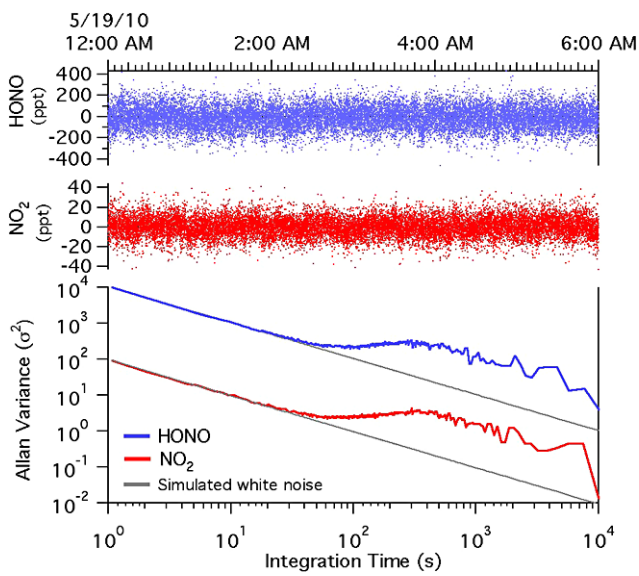

Fig. 3 The *top two panels* show HONO (*blue*) and NO_2 (*red*) mixing ratios in ppt (pmol/mol) measured in zero-air at 40 torr. The Allan variance plot *on the bottom panel* shows the decrease in instrument variance with time averaging for both species. Deviation from pure white or random noise occurs due to slow-moving temperature-driven optical fringes, but is addressed with frequent spectral background subtractions, here conducted every fifth minute for 30 seconds (20 seconds to obtain an average background spectrum and 10 seconds of flush time). The *y*-intercepts on the Allan variance plot representing the 1-second 1σ measurement noise for HONO and NO_2 are 9.4×10^3 and 8.8×10^1 $ppt^2\,Hz^{-1}$, or 97 and 9.4 $ppt\,Hz^{-1/2}$, respectively

3 Line-strengths

The accuracy of the mixing ratios obtained using absorption spectroscopy largely depends on the accuracy of the absorption cross-section or line-strength. For long-lived gases and other well-studied species such as NO_2, the absorption parameters are well characterized and available in publications and in databases such as HITRAN [18]. For HONO, however, there are fewer published studies and greater uncertainty in absolute values, which required us to re-evaluate the HONO spectra.

We determined the amount of infrared (1659.1 to 1660.2 cm^{-1}) light absorbed by the *cis* conformer of HONO while sampling a known amount of total (*cis* + *trans*) HONO at the given constant temperature of 303 K, hence at a constant *cis* to *trans* ratio. This *effective* line-strength of *cis*-HONO was obtained by introducing high levels of gaseous HONO (between 300 and 800 ppb)—generated by passing HCl vapor over powdered $NaNO_2$ [23]—into the sampling cell at low pressures (<9 torr) to minimize absorption line overlap while maintaining high signal to noise. In parallel, we quantitatively converted the same HONO source to NO using a heated molybdenum catalyst and quantified NO with a pulsed-mode QC laser (1906.73 cm^{-1}, Hamamatsu Photonics) spectrometer calibrated against a traceable NO standard to determine the absolute HONO concentration. Because NO is relatively inert, it is less susceptible to line-losses and can be accurately calibrated using traceable gas mixtures.

Deviation of the sample from the temperature at which our effective line-strengths were determined will result in a change in the *cis* to *trans* ratio. The effective line-strengths can be corrected knowing the *cis-trans* energy barrier, for which there is a large discrepancy amongst reported values [24–28]. In practice, a constant sample temperature is well maintained by heating the inlet, tubing, the optical table and its protective cover. Furthermore, routine calibration gas additions are conducted in the field to ensure the accuracy of the measurements, as discussed in the next section. Lastly, because the time required for isomerization to occur is much shorter ($\sim 10^{-12}$ seconds) than that needed for ambient air to travel through the inlet and subsequent tubing to the sampling cell ($\sim$1 second), we expect the HONO conformers to be in thermal equilibrium and independent of changing ambient conditions.

Line positions and effective line-strengths used in the spectral fits in Fig. 2 are listed in Table 1. Additional details regarding this experiment, along with comparison of the relative absorption strengths between *cis* and *trans* conformers, determination of the pressure-broadening coefficient, comparison to values in the ATMOS database and to a high-resolution FTIR spectrum are part of an ongoing analysis that is not yet complete.

Table 1 Peak position and *effective* line-strength of *cis*-HONO between 1659.5 and 1659.7 cm^{-1} measured at 303 K

Peak position (cm^{-1})	Effective line-strength (cm^2 $molecule^{-1}$ cm^{-1}) $\times 10^{-21}$
1659.5031	9.571
1659.5099	8.810
1659.5887	10.15
1659.5968	3.283
1659.6238	1.863
1659.6770	12.92
1659.6886	7.419

4 Sampling technique

Figure 4 shows a schematic of the inlet manifold we use for minimizing contact between sampled ambient air and moist surfaces, for removing coarse particles by inertial separation and for routine additions of reference gases and zero-air. HONO (Henry's Law constant, $K_H = 50$ M atm^{-1})—though not nearly as soluble as HNO_3 ($K_H = 2.1 \times 10^5$ M atm^{-1})—is still photo-chemically active, relatively soluble compared to NO (1.4×10^{-3} M atm^{-1}) and NO_2 (1.2×10^{-2} M atm^{-1}), and mostly dissociated above pH 3.3 [29–32]. In addition to the high probability of HONO equilibrating with accumulated particles and moist surfaces, there is strong evidence for heterogeneous reactions converting precursors to HONO [33]. Consequently, both positive and negative HONO artifacts are a concern, leading us to minimize opportunities for the sample to contact humid surfaces and aerosol that would accumulate on a particle filter.

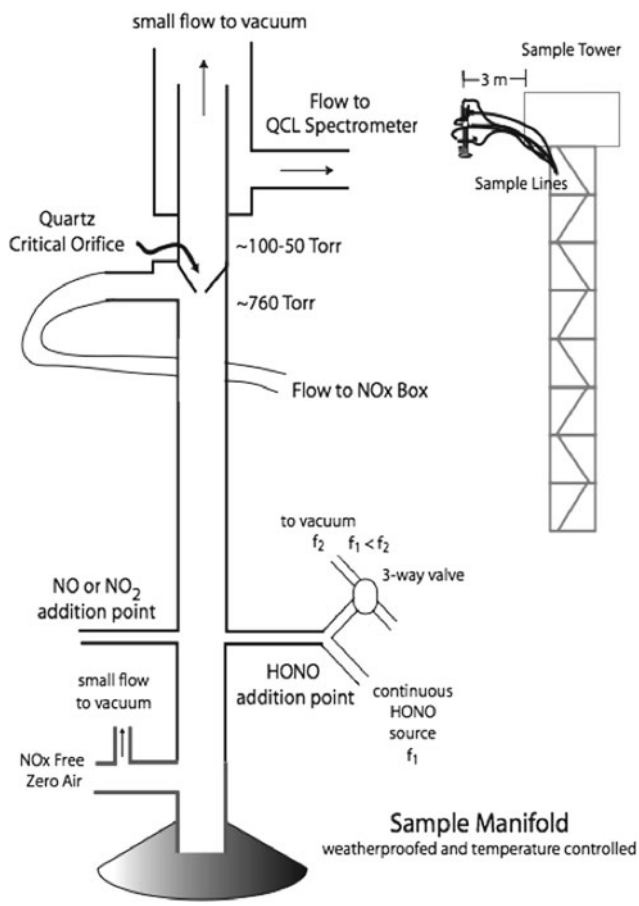

Fig. 4 Schematic of the quartz inlet manifold. The inlet and subsequent tubing are shielded from light to prevent photolysis and photo-induced surface reactions

Surface-adsorbed water is minimized by (1) using a siloxyl-coated quartz inlet to make its surface hydrophobic, (2) heating the inlet, the downstream tubing and sampling cell and (3) reducing the pressure by drawing the sample through a critical orifice built into the inlet (Fig. 4). The divergent flows after the orifice—with exhaust vented in line with the incoming flow and the sample air forced to make a 180° turn—cause particles with diameters 4 μm or larger to be separated out of the sample flow by inertia [34, 35]. The inlet and subsequent tubing are shielded from light to avoid photolytic losses and photo-enhanced reactions involving surface-adsorbed nitrate ions leading to HONO production [33]. A similarly designed inlet was used successfully to measure formaldehyde, formic acid and ammonia, which are also highly surface active [36, 37].

Frequent in-field artifact testing is an integral part of the instrument system. The manifold is equipped with ports at the entrance of the inlet to allow for routine additions of standards and zero-air (Fig. 4). An outlet adjacent to the flow-restricting orifice is used to draw a subsample of the ambient matrix to a heated Mo catalyst to convert all reducible nitrogen oxides to NO, followed by quantification of the NO by O_3-chemilumiscence. HONO generated from the HCl + $NaNO_2$ source, which typically is >97% pure, is dynamically mixed with zero-air, added at the inlet entrance in excess of the total sample flow-rate and sampled by both instruments, thereby providing an independent check on the measurements by tying the observations to traceable NO standards. A similar test is applied for NO_2, which is supplied from either compressed gas standards or a permeation tube.

Standard gas additions can also test for temporary surface adsorption that attenuates atmospheric variations. The rise and fall in absorbance when a standard is switched on or off should be nearly instantaneous, with only some delay associated with the flushing time defined by the pumping speed through the inlet, tubing and sampling cell as well as smearing due to mixing and diffusion. These response times can be determined by fitting the mixing ratio time series during standard gas additions to a single exponential curve. A slower response of HONO compared to that of an inert gas would suggest some uptake of HONO on the

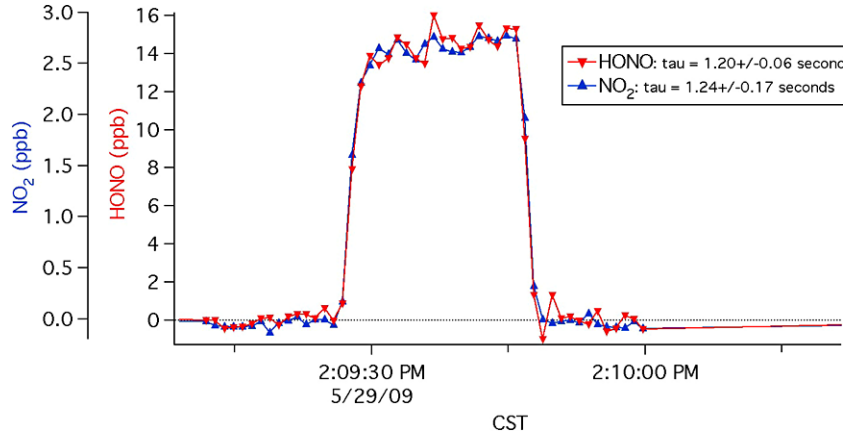

Fig. 5 One-second mixing ratios of HONO and NO_2 during calibration gas additions, observed during the Study of Houston Atmospheric Radical Precursor (SHARP) campaign in April and May of 2009. The response times (tau)—determined by the pumping speed and cell volume (5 L)—of HONO and NO_2 are indistinguishable, indicating no preferential loss of HONO through the inlet, tubing and sampling cell

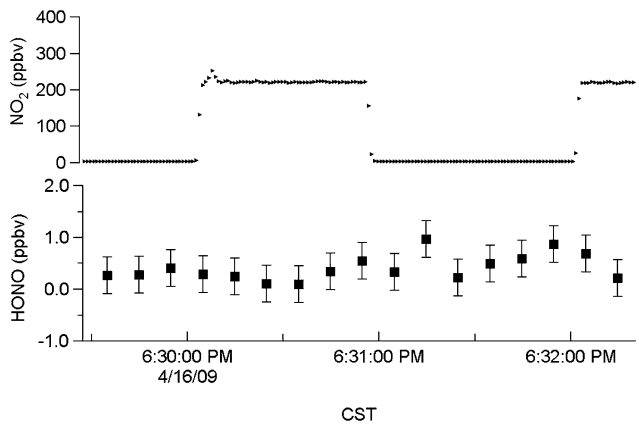

Fig. 6 One-second mixing ratios of NO_2 (*top*) and ten-second average mixing ratios of HONO (*bottom*) during a high-concentration NO_2 addition through 40-feet (12.2 m) of unheated tubing at ambient pressure, conditions under which surface reactions are favored. Note that there is no HONO formed during or immediately following high levels of NO_2 under humid conditions (no positive artifact). The error bars represent the standard deviation of 10-second averaged data

surfaces. For the current instrumental configuration, HONO response is compared to that of NO_2, which also is generally not attenuated by wall interactions [15–17]. A prototype of this inlet system was deployed at the Study of Houston Atmospheric Radical Precursor (SHARP) campaign in April and May 2009, during which polluted, humid air was sampled through the inlet and 40 ft (12.2 m) of 3/8″ O.D. (9.5 mm) PFA Teflon tubing. Figure 5 shows indistinguishable response times between HONO and NO_2 during additions of both gases at SHARP.

The possibility for positive artifacts from the inlet, tubing or cell surface reactions forming HONO is checked by introducing NO_2 into the inlet in addition to the ambient air matrix. An increase in HONO mixing ratios during these additions would indicate reactions involving NO_2 yielding HONO. During the SHARP campaign, we did not observe any artifact HONO when NO_2 was added to ambient air (Fig. 6). Even at NO_2 levels exceeding 100 ppb—well above the range of observed values—there was no change in the HONO mixing ratio, demonstrating freedom from positive artifacts based on NO_2.

Figure 7 shows the mixing ratios of HONO and NO_2 measured during the SHARP campaign. The levels of the two species typically co-vary in time as a result of common or co-located emission sources and mixing in the atmosphere. Higher levels are usually observed in the early morning and in the evening when weaker vertical mixing and shallow boundary layer heights promote accumulation of pollutants and photo-chemical losses are reduced compared to mid-day conditions.

5 Conclusions

This dual continuous-wave mode quantum cascade laser spectrometer has achieved one-second detection limits (S/N = 3) for HONO and NO_2 of 300 and 30 ppt, respectively. Spectral averaging with frequent background subtractions allows further reduction in signal noise, improving the HONO and NO_2 detection limits (S/N = 3) to 35 and 3 ppt, respectively, over a 30-minute integration period. The detection limit for HONO is higher than that for NO_2—despite better absorbance precision on this channel—due to much weaker line-strengths for *cis*-HONO between 1659 and 1660 cm^{-1} compared to NO_2 at 1604 cm^{-1}. A sample-handling scheme that minimizes adsorbed water on the inlet and subsequent tubing that bring sample into the optical cell is effective at preventing both positive and negative HONO artifacts. The system is designed to allow inlet checks to be a part of routine field operation and provide frequent quality checks on the measurement.

The instrument described in this study was adapted from a previously deployed instrument with a large optical table and near 1 m base-length multi-pass cell. With insulation and a protective cover, the instrument is 3 ft × 6 ft (0.9 m × 1.8 m). The performance demonstrated by this implementation points to the possibility of using a re-designed

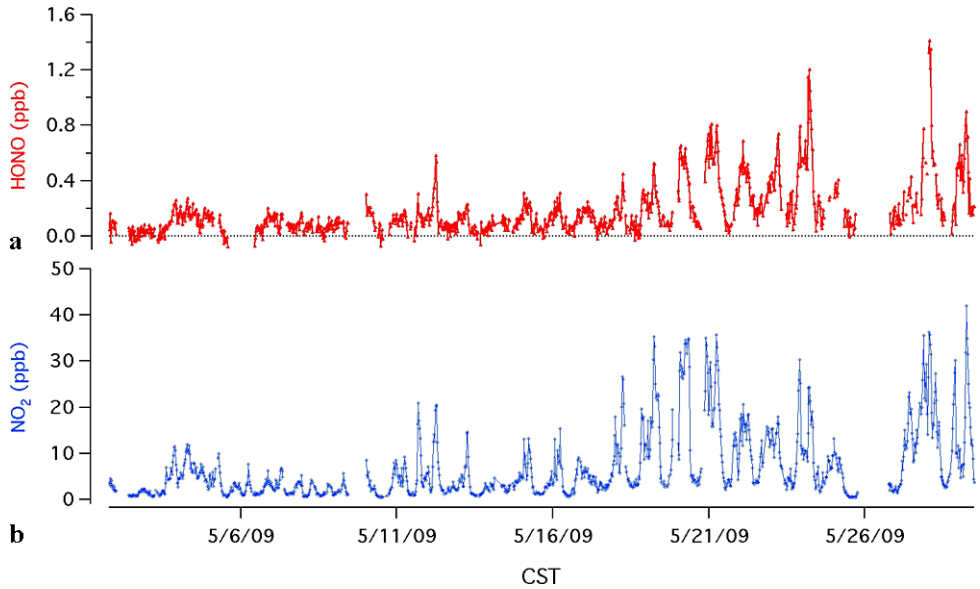

Fig. 7 Observed 30-minute averaged mixing ratios in ppb (nmol/mol) of HONO (**a**) and NO_2 (**b**) during the entire SHARP campaign. Gaps in the data are due to maintenance operations, inlet attenuation/artifact tests and instrument shutdown from power failures

astigmatic multi-pass cell with a base-length of 47.5 cm and 200 m of absorption path-length. This cell fits on an optical table measuring 43 × 65 cm. Its smaller volume of 2.1 L allows faster response times and will be more easily portable for field use without any sacrifice in detection limit [38].

The chief advantages of this dual cw-QC TILDAS spectrometer over previous diode laser and pulsed-mode QC laser systems are higher power output and narrower laser line-widths, which provide improved precision and enable thermo-electrically cooled detectors to be used instead of cryogenically cooled detectors that present logistical challenges for long-term, remote operation in the field. This spectrometer has been deployed at a rural forest to measure the diurnal and seasonal trends in the exchange of HONO and NO_2 between the biosphere and atmosphere.

Acknowledgements The authors gratefully acknowledge the assistance of Ryan McGovern, Stanley Huang and Daniel Glen of Aerodyne Research, Inc., Josh McLaren and Bruce Daube of Harvard University, and the entire SHARP research team. This work was supported by the National Science Foundation Awards No. AGS—0813617 and 0814202. Additional funding for the SHARP campaign was provided by the Houston Advanced Research Center Grant No. H113.

References

1. B. Alicke et al., J. Geophys. Res., Atmos. **108** (2003)
2. W. Liao et al., Geophys. Res. Lett. **33** (2006)
3. X.L. Zhou et al., J. Geophys. Res., Atmos. **112** (2007)
4. S.S. Park et al., Atmos. Environ. **42**, 6586 (2008)
5. M. Sleiman et al., Proc. Natl. Acad. Sci. USA **107**, 6576 (2010)
6. J. Kleffmann et al., Atmos. Environ. **40**, 3640 (2006)
7. J.E. Dibb et al., Atmos. Environ. **38**, 5399 (2004)
8. J. Heland et al., Environ. Sci. Technol. **35**, 3207 (2001)
9. X.L. Zhou et al., Environ. Sci. Technol. **33**, 3672 (1999)
10. J. Kleffmann, P. Wiesen, Atmos. Chem. Phys. **8**, 6813 (2008)
11. R. Kurtenbach et al., Atmos. Environ. **35**, 3385 (2001)
12. U. Platt et al., Nature **285**, 312 (1980)
13. Y.Q. Li, J.J. Schwab, K.L. Demerjian, Geophys. Res. Lett. **35** (2008)
14. C.L. Schiller et al., J. Atmos. Chem. **40**, 275 (2001)
15. C.V. Horii et al., J. Geophys. Res., Atmos. **109** (2004)
16. C.V. Horii et al., Agric. For. Meteorol. **133**, 210 (2005)
17. C.V. Horii et al., Proc. SPIE **3758**, 152 (1999)
18. L.S. Rothman et al., J. Quant. Spectrosc. Radiat. Transf. **96**, 139 (2005)
19. J.B. McManus, Appl. Opt. **46**, 472 (2007)
20. J.B. McManus et al., Appl. Phys. B, Lasers Opt. **85**, 235 (2006)
21. D.D. Nelson et al., Appl. Phys. B, Lasers Opt. **75**, 343 (2002)
22. M.S. Zahniser et al., Proc. SPIE **7222, 72220H** (2009)
23. A. Febo et al., Environ. Sci. Technol. **29**, 2390 (1995)
24. A. Bongartz et al., J. Phys. Chem. **95**, 1076 (1991)
25. L.H. Jones, R.M. Badger, G.E. Moore, J. Chem. Phys. **19**, 1599 (1951)
26. G.E. Mcgraw, D.L. Bernitt, I.C. Hisatsun, J. Chem. Phys. **45**, 1392 (1966)
27. V. Sironneau et al., J. Mol. Spectrosc. **259**, 100 (2010)
28. R. Varma, R.F. Curl, J. Phys. Chem. **80**, 402 (1976)
29. K.H. Becker et al., J. Phys. Chem. **100**, 14984 (1996)
30. W.L. Chameides, J. Geophys. Res., Atmos. **89**, 4739 (1984)
31. J. Goretski, O.C. Zafiriou, T.C. Hollocher, J. Biol. Chem. **265**, 11535 (1990)
32. J. Lelieveld, P.J. Crutzen, J. Atmos. Chem. **12**, 229 (1991)
33. X.L. Zhou et al., Geophys. Res. Lett. **29** (2002)
34. B.W. Loo, C.P. Cork, Aerosol Sci. Technol. **9**, 167 (1988)
35. V.A. Marple, C.M. Chien, Environ. Sci. Technol. **14**, 976 (1980)
36. R.A. Ellis et al., Atmos. Meas. Tech. **3**, 397 (2010)
37. S.C. Herndon et al., J. Geophys. Res., Atmos. **112** (2007)
38. J.B. McManus et al., Opt. Eng. **49** (2010)